

Velocity-Space Proton Diffusion in the Solar Wind Turbulence

Y. Voitenko¹ · V. Pierrard^{1,2}

Published in ArXiv 3 April 2013

© ••••

Abstract We study a velocity-space quasilinear diffusion of the solar wind protons driven by oblique Alfvén turbulence at proton kinetic scales. Turbulent fluctuation at these scales possess properties of kinetic Alfvén waves (KAWs) that are efficient in Cherenkov resonant interactions. The proton diffusion proceeds via Cherenkov kicks and forms a quasilinear plateau - nonthermal proton tail in the velocity distribution function (VDF). The tails extend in velocity space along the mean magnetic field from 1 to $(1.5-3) V_A$, depending on the spectral break position, turbulence amplitude at the spectral break, and spectral slope after the break. The most favorable conditions for the tail generation occur in the regions where the proton thermal and Alfvén velocities are about the same, $V_{Tp}/V_A \approx 1$. The estimated formation times are within 1–2 h for typical tails at 1 AU, which is much shorter than the solar wind expansion time. Our results suggest that the nonthermal proton tails, observed in-situ at all heliocentric distances > 0.3 AU, are formed in the solar wind locally by the KAW turbulence. We also suggest that the bump-on-tail features - proton beams, often seen in the proton VDFs, can be formed at a later evolution stage of the nonthermal tails by the time-of-flight effects.

Keywords: Solar wind; Waves; Turbulence; Space Plasmas

1. Introduction

Low collisionality of the solar wind (SW) and persistent activity of waves and turbulence make kinetic wave-particle interactions unavoidable in the SW modeling. The need for such kinetics has been emphasized in view of numerous non-thermal features observed in velocity distribution functions (VDFs) of the solar wind particles (see Marsch (2006) and references therein). In particular,

¹ Solar-Terrestrial Centre of Excellence, Space Physics
Division, Belgian Institute for Space Aeronomy,
Ringlaan-3-Avenue Circulaire, B-1180 Brussels, Belgium,
email: yuriy.voitenko@oma.be

² Georges Lemaître Centre for Earth and Climate Research
(TECLIM), Université Catholique de Louvain, Place Louis
Pasteur 3, bte L4.03.08, 1348 Louvain-la-Neuve, Belgium

nonthermal tails, beams, and temperature anisotropies are routinely observed in situ by satellites.

Recent in-situ measurements have revealed that the SW turbulence at proton kinetic scales is dominated by Alfvénic waves (AWs) rather than the fast mode or whistler waves (He *et al.*, 2011, 2012; Podesta and Gary, 2011). Furthermore, among Alfvén waves, the most power, about 80%, was found in oblique quasi-perpendicular AWs, and the rest 20% in the quasi-parallel ion-cyclotron Alfvén waves (ICAW) (He *et al.*, 2011).

Properties of quasi-parallel ICAWs are understood much better than that of the oblique AWs at proton kinetic scales. ICAWs experience strong ion-cyclotron resonances and are considered as a main source for the perpendicular heating of the protons and heavier ions in the solar corona and solar wind (see reviews by Hollweg and Isenberg (2002), Marsch (2006) and references therein).

Properties of the dominant quasi-perpendicular AW fraction and its influence on particles VDFs are still unclear. Depending on the wavevector anisotropy k_{\perp}/k_{\parallel} (perpendicular/parallel with respect to the mean magnetic field B_0), less oblique AWs at proton kinetic scales are similar to ICAWs, while more oblique AWs are kinetic Alfvén waves (KAWs). At intermediate $k_{\perp}/k_{\parallel} \approx V_A/V_{Tp}$, AWs possess mixed properties of both ICAWs and KAWs and can be named ion-cyclotron KAWs - ICKAWs (Voitenko and Goossens, 2003). Since ICKAWs experience both the ion-cyclotron resonance (typical for ICAWs) and the Cherenkov resonance (typical for KAWs), they have more dissipation and generation channels and can play an important role in the energy exchange between parallel and perpendicular degrees of freedom in the solar wind.

The wavevector anisotropy at proton kinetic scales has been measured by Sahraoui *et al.* (2010). For perpendicular wave numbers up to $k_{\perp}\rho_p \simeq 2$, the wave/proton-cyclotron frequency ratio appeared to be still low, $\omega/\Omega_p \simeq 0.1$, whereas the anisotropy is high, about $k_{\perp}/k_{\parallel} \simeq 10$, which is typical for classic KAWs. The dominant role of KAWs in the oblique AW fraction has been supported further by two independent tests performed by Salem *et al.* (2012), who measured simultaneously two polarization ratios: compressional magnetic/total magnetic and total electric/total magnetic field perturbations.

The interest in KAWs and related issues has risen recently in the context of turbulence dissipation in the solar wind and consequent heating of plasma species (Schekochihin *et al.* (2009); Howes (2011); and references therein). Goldreich and Sridhar (1995) suggested that the MHD AW turbulence cascades along a critical balance path, which result in preferential generation of high perpendicular wavenumbers, and hence KAWs (Schekochihin *et al.*, 2009). An indirect confirmation of the critical balance was received recently by Gogoberidze, Chapman, and Hnat (2012), who proved that the critical balance leads to generation of the residual energy observed in the solar wind turbulence.

A solar wind model elaborating Landau damping of KAWs has predicted the electron and proton heating rates (Howes, 2011), which agree well with empirical estimations by Cranmer *et al.* (2009) at $\gtrsim 0.8$ AU. At smaller radial distances the proton heating by Landau damping appeared to be insufficient and Howes (2011) suggested the proton cyclotron heating operating there. Because of the shorter inertial range, the MHD turbulence at shorter radial distances ends up

with less anisotropic fluctuations at proton kinetic scales, which can produce the required proton heating via cyclotron resonant interaction.

A widely used assumption of the Maxwellian Landau damping can be violated in the solar wind by local deformations of VDFs of particles in resonant velocity ranges. Borovsky and Gary (2011) have demonstrated that the electron Landau damping is still strong (although not Maxwellian any more) because the relatively high collisionality of the electron is capable of keeping their VDFs not far from Maxwellian. On the contrary, the less collisional protons experience much stronger departures from Maxwellian VDFs, which can significantly modify the proton Landau damping, or even cancel it.

Chandran *et al.* (2010) proposed another promising heating mechanism for the protons, stochastic acceleration by KAWs across B_0 . This mechanism is not related to the kinetic wave-particle resonances, and is therefore not so sensitive to the local deformations of the proton VDFs.

If the turbulence at proton kinetic scales consists of the ion-cyclotron and KAW fractions, as is suggested by recent observations, both these fractions should produce their own observed signatures - specific features in the proton VDFs. The most typical observed features of the proton VDFs are (Marsch, 1991): (i) nonthermal tails or even secondary peaks along the magnetic field direction in all solar wind types (fast, slow, and intermediate), and (ii) total temperature anisotropies $T_{p\perp} > T_{p\parallel}$ in the fast solar wind (with anisotropic proton cores), and $T_{p\parallel} > T_{p\perp}$ in the slow (with isotropic cores) and intermediate (with both isotropic and anisotropic cores) solar winds. The parallel proton tails and beams are important contributors to the energy balance between parallel and perpendicular degrees of freedom. In the fast solar wind they reduce the total temperature anisotropy to $T_{p\perp}/T_{p\parallel} \gtrsim 1$ (and at times even reverse to $T_{p\parallel} > T_{p\perp}$) despite the strongly anisotropic cores of the proton VDFs, $T_{p\perp}^{\text{core}}/T_{p\parallel}^{\text{core}} = 2 - 3$ (see Figure 8.4 by Marsch, 1991). In the intermediate and slow solar wind they dominate the energy balance making $T_{p\parallel}/T_{p\perp} > 1$. Among them, the nonthermal tails prevail (Marsch *et al.*, 1982). The secondary peaks (bumps-on-tails) are less frequent and develop on the tail background mainly in the fast solar wind. Therefore the bump-on-tail seems to be a later evolution stage of the proton VDF as compared to the tail. At the same time, persistent nonthermal tails without bumps are observed at all distances, which suggest that the bumps are not necessary developing on the tails within the solar wind expansion time-scale; their development is therefore somehow constrained or require more time.

The anisotropic cores of the proton VDFs with $T_{p\perp}^{\text{core}} > T_{p\parallel}^{\text{core}}$ have been associated with the ion-cyclotron heating by ion-cyclotron resonant waves, and ICAWs interaction with solar wind protons and heavier ions have been studied extensively (Hollweg and Isenberg (2002); Marsch (2006); and references therein). It was in particular shown that the ion-cyclotron pitch-angle diffusion can be responsible for the shaping and perpendicular heating of the core proton VDFs (Marsch and Tu, 2001), for the cross-field heating of heavier ions (Galinsky and Shevchenko, 2012), and also for the pitch-angle scattering of the nonthermal proton tails (Marsch and Bourouaine, 2011).

Wave mechanisms producing nonthermal proton tails and bumps-on-tails (beams) in the solar wind received much less attention. The first one, proposed

by Tu, Wang, and Marsch (2002), relied upon the proton cyclotron-resonant diffusion driven by a specific ion-cyclotron mode supported by helium ions. Another mechanism, nonlinear proton trapping in the parallel KAW potentials, has been suggested by Voitenko and Goossens (2006). Later on, analytical (Pierrard and Voitenko, 2010) and numerical (Li *et al.*, 2010; Osmame, Hamza, and Meziane, 2010) studies have confirmed that a KAW with reasonable amplitude can produce observed proton beams in the solar wind conditions.

Proton trapping and beam generation can also be produced by electrostatic waves carrying parallel electric fields. Recent simulations of the nonlinear decay of circularly polarized Alfvén waves have demonstrated that the product electrostatic waves can trap and accelerate protons along B_0 , thereby creating a beam (Araneda, Marsch, and Vinas, 2008; Matteini *et al.*, 2011; Valentini, Perrone, and Veltri, 2011). Ion-acoustic waves (Araneda, Marsch, and Vinas, 2008; Matteini *et al.*, 2011) and "ion-bulk" waves (Valentini, Perrone, and Veltri, 2011) have been discussed as mediators transferring energy from AWs to plasma particles. Alternatively, Rudakov *et al.* (2012) used a quasilinear approach to study the proton diffusion driven by a strongly dispersive KAW spectrum. This process can produce a quasilinear plateau in the form of nonthermal tail in the proton VDF.

Earlier kinetic models of the SW electrons, accounting for the influence of external macroscopic forces and Coulomb collisions (Pierrard, Maksimovic, and Lemaire, 1999; Lie-Svendsen and Leer, 2000; Vocks and Mann, 2009), have been recently improved by the inclusion of terms due to whistler turbulence (Pierrard, Lazar, and Schlickeiser, 2011). It was concluded that the whistler turbulence, if exists in the solar wind, could lead to the velocity-space diffusion of electrons and form nonthermal tails in the electron VDF. Another source for the velocity-space electron diffusion has been studied by Rudakov *et al.* (2011), who assumed a spectrum of kinetic Alfvén waves (KAWs) instead of whistlers. Moreover, Rudakov *et al.* (2011) argued that the nonlinear KAW scattering off electrons is more efficient than the nonlinear wave-wave interaction in the short-wavelength KAW range.

In the present paper we study the influence of the observed kinetic-scale turbulence on the evolution of the proton VDF. First we derive the Fokker-Planck diffusion terms for protons under the action of Alfvénic turbulence. We are interested here in the influence of the KAW component, which is dominant in the kinetic-scale SW turbulence, on the evolution of the proton VDF. The Fokker-Planck diffusion coefficients are presented in terms of quantities measured in-situ in the solar wind. In particular we refer to magnetic field measurements that provided spectral indexes of the SW turbulence at proton kinetic scales (Alexandrova *et al.*, 2009; Sahraoui *et al.*, 2010), MHD/kinetic spectral break wavenumber, and the turbulence amplitude at the break wavenumber (Smith *et al.*, 2006; Markovskii, Vasquez, and Smith, 2008). Analytical and numerical estimations are given for the evolution of nonthermal tails in the proton VDFs.

2. Wave Model

The classic KAW dispersion can be presented as

$$\omega_k = k_{\parallel} V_A K, \quad (1)$$

where \mathbf{k} is the wave vector, \parallel (\perp) mean components parallel(perpendicular)to \mathbf{B}_0 , $K = K(\mu)$ is the KAW dispersion function, and $\mu = \rho_p k_{\perp}$ is the dimensionless perpendicular wavenumber.

The kinetic dispersion function for KAWs was derived by Hasegawa and Chen (1976):

$$K = \mu \sqrt{\frac{1}{1 - \Lambda_0} + \frac{T_{e\parallel}}{T_{p\perp}}}, \quad (2)$$

where $\Lambda_0 = \Lambda_0(\mu) = I_0(\mu^2) \exp(-\mu^2)$, $I_0(\mu^2)$ is the zero-order modified Bessel function, and $T_{e(p)}$ is the electron(proton) temperature. This expression was obtained in the following wave and plasma parameter ranges: $k_{\parallel}^2/k_{\perp}^2 \ll 1$, $\omega_k^2/\Omega_p^2 \ll 1$, $V_{Tp}^2 \ll V_A^2 \lesssim (\omega_k/k_{\parallel})^2 \ll V_{Te}^2$.

The KAW dispersion function gives the KAW phase velocity, $V_k = \omega_k/k_{\parallel}$, in units of Alfvén velocity: $V_k/V_A = K(\mu)$. In the MHD limit $\mu \rightarrow 0$ KAWs become dispersiveless Alfvén waves, $V_k \rightarrow V_A$, but with growing μ the KAW phase velocity deviates from the Alfvén velocity significantly. The inverse function $K^{-1}(V_k/V_A)$, which we will need later in the diffusion coefficient, is impossible to find from Equation (2) analytically in general case. Explicit expressions for $K^{-1}(V_k/V_A)$ can only be found in two asymptotic regimes of weak ($\mu^2 \ll 1$) and strong ($\mu^2 \gg 1$) wave dispersion.

To simplify the problem, one can use a Padé approximation for $\Lambda_0(\mu)$,

$$\Lambda_0(\mu) \simeq \frac{1}{1 + \mu^2}, \quad (3)$$

resulting in the following KAW dispersion function

$$K \simeq K_P = \sqrt{1 + \left(1 + \frac{T_{e\parallel}}{T_{p\perp}}\right) \mu^2} \quad (4)$$

and its derivative

$$\partial K_P / \partial \mu = \left(1 + \frac{T_{e\parallel}}{T_{p\perp}}\right) \frac{\mu}{K_P}. \quad (5)$$

These expressions can also be found in the framework of two-fluid MHD plasma model and provide a good approximation for KAWs in the whole range of μ if the plasma beta $\beta = (1 + T_{e\parallel}/T_{p\perp}) V_{Tp}^2/V_A^2 \ll 1$. As is seen from Figure 1, the difference between the kinetic KAW dispersion $K(\mu)$ (solid line) and its' Padé approximation $K_P(\mu)$ (dashed line) is insignificant for $T_{e\parallel}/T_{p\perp} \approx 1$.

Finite- β effects come into play in the solar wind at 1 AU, where the typical value $\beta \approx 1$ (this corresponds to the plasma/magnetic pressure ratio ≈ 1). The

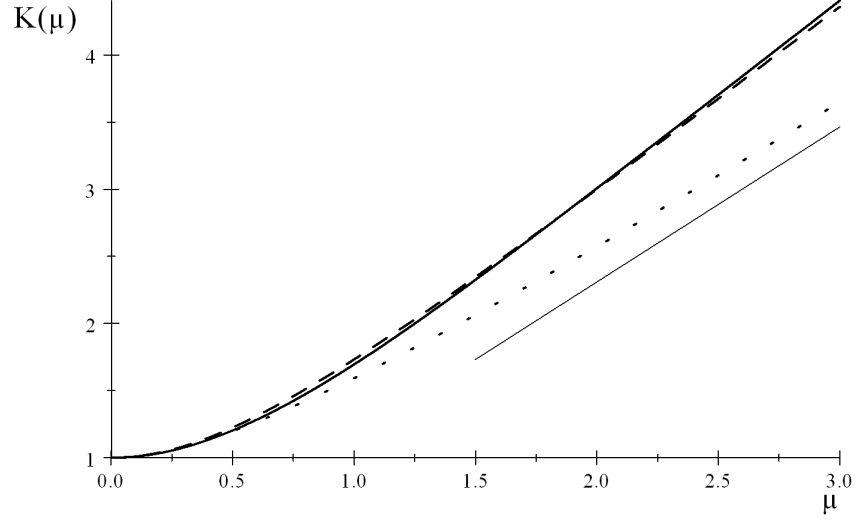


Figure 1. Comparison of three models for the KAW dispersion function $K(\mu)$: (1) kinetic dispersion by Hasegawa and Chen (1976) for $\beta \ll 1$ (solid line); (2) Padé approximation, that corresponds to the two-fluid MHD dispersion for $\beta \ll 1$ (dash line); (3) two-fluid dispersion with finite- β effects for $\beta_{\parallel} = \beta_{\perp} = 0.5$ (dot line) and its asymptote (bottom solid line). In all cases $T_{e\parallel}/T_{p\perp} = 1$.

KAW dispersion function K_{β} , accounting for the finite- β effects of magnetic and plasma compressibility (Voitenko and Goossens, 2002), can be modified for the case of anisotropic temperatures:

$$K_{\beta}^2 = \frac{1 + \frac{\beta_{\parallel}}{1+\beta_{\perp}} + \frac{1+T_{e\parallel}/T_{p\perp}}{1+\beta_{\perp}}\mu^2}{2} + \sqrt{\left(\frac{1 + \frac{\beta_{\parallel}}{1+\beta_{\perp}} + \frac{1+T_{e\parallel}/T_{p\perp}}{1+\beta_{\perp}}\mu^2}{2}\right)^2 - \frac{\beta_{\parallel}}{1+\beta_{\perp}}}, \quad (6)$$

where $\beta_{\parallel,\perp} = (1 + T_{e\parallel,\perp}/T_{p\parallel,\perp}) V_{Tp\parallel,\perp}^2/V_A^2$. This dispersion is also shown in Figure 1 (dot line). The corresponding KAW wavenumber μ can be expressed via V_k explicitly,

$$\mu = \sqrt{\frac{1 + \beta_{\perp}}{1 + T_{e\parallel}/T_{p\perp}} \frac{\left(\frac{V_k}{V_A}\right)^4 - \left(1 + \frac{\beta_{\parallel}}{1+\beta_{\perp}}\right) \left(\frac{V_k}{V_A}\right)^2 + \frac{\beta_{\parallel}}{1+\beta_{\perp}}}{\left(\frac{V_k}{V_A}\right)^2}}. \quad (7)$$

At large μ , the KAW dispersion (phase velocity) can be decreased significantly by the finite- β effects. On the contrary, in the weakly dispersive range $\mu < 1$ such moderate values as $\beta = 0.5$ do not change the KAW dispersion significantly

and can be approximated there as

$$\mu = K_p^{-1} \left(\frac{V_k}{V_A} \right) = \sqrt{\frac{\left(\frac{V_k}{V_A} \right)^2 - 1}{1 + \frac{T_{e\parallel}}{T_{p\perp}}}}. \quad (8)$$

3. Proton Diffusion in the KAW Turbulence

The parallel component of the KAW electric field $E_{z\mathbf{k}}$ ($\mathbf{k} = (k_x, k_y, k_z)$ is the wave vector, $\mathbf{z} \parallel \mathbf{B}_0$), makes KAWs efficient in Cherenkov interaction with plasma particles. Following (Voitenko, 1998; Voitenko and Goossens, 2003), we account for the proton VDFs modifications under the action of KAWs in the framework of quasi-linear theory. We consider an axially symmetric (with respect to the background magnetic field \mathbf{B}_0) problem, where both the KAW spectrum and the particle velocity distributions are independent of respective polar angles in the cross-field plane.

In general, the proton distribution function $F = F(\mathbf{r}, \mathbf{V}, t)$ in the solar wind obeys the Vlasov collisional equation

$$\left(\frac{\partial}{\partial t} + \mathbf{V} \cdot \frac{\partial}{\partial \mathbf{r}} + \mathbf{a} \cdot \frac{\partial}{\partial \mathbf{V}} \right) F = \left(\frac{dF}{dt} \right)_C + \left(\frac{dF}{dt} \right)_A, \quad (9)$$

where \mathbf{r} and \mathbf{V} are respectively the position and velocity vectors of the protons, t is the time, and \mathbf{a} is the proton acceleration under the action of the external forces: the macroscopic electric force $Ze\mathbf{E}_0$, the gravitational force $m\mathbf{g}$ and the Lorentz force $\propto \mathbf{v} \times \mathbf{B}_0$. The right-hand side represents the velocity-space proton diffusion due to Coulomb collisions, $(dF/dt)_C$, and due to wave-particle collisions,

$$\left(\frac{dF}{dt} \right)_A = \frac{\partial}{\partial V_z} D^A \frac{\partial F}{\partial V_z}.$$

In the diffusion coefficient D^A we integrate over the polar angles in the cross- \mathbf{B}_0 plain, implying that $|E_{z\mathbf{k}}|^2$ is axially symmetric, but we keep the dependence on the perpendicular component of the particle velocity:

$$D^A = \frac{\pi q_p^2}{2m_p^2} \sum_{\mathbf{k}} \delta(\omega_k - k_z V_z) J_0^2 |E_{z\mathbf{k}}|^2 \quad (10)$$

where the zero-order Bessel function $J_0 = J_0(k_\perp \rho_p V_\perp / V_{Tp})$ reflects the fact that the actual electric field of KAWs acting on the protons is reduced because of the averaging over their cyclotron orbits with the velocity-dependent gyroradius $V_\perp / \Omega_p = \rho_p V_\perp / V_{Tp}$. Other notations are as follows: k_z and k_\perp are the wave vector components parallel and perpendicular to B_0 , $k_\perp^2 = k_x^2 + k_y^2$, $\rho_p = V_{Tp} / \Omega_p$ is the proton gyroradius, $V_{Tp} = \sqrt{T_p / m_p}$ thermal velocity, T_p temperature, m_p proton mass, q_p proton charge, and $\sum_{\mathbf{k}} = 2\pi \int dk_z \int dk_\perp k_\perp$. Dirac's delta-function $\delta(\omega_k - k_z V_z)$ follows from the resonant character of the Cherenkov wave-particle interaction.

The simplest solar wind models consider only the effects of the external forces. In such models called exospheric, the right-hand side interaction terms in Equation (9) are neglected so that an analytic solution of the equation can be obtained (Lamy *et al.* (2003) and reference therein). Coulomb collisions make equations too complex and require numerical simulations. Expressions for the Coulomb diffusion term in the Vlasov equation for protons and results of numerical simulations accounting for Coulomb collisions are presented in (Pierrard and Voitenko, 2012). ■

Starting from Equation (10), the wave-particle diffusion term accounting for turbulence properties is derived in next sections. We especially pay attention to a non-monotonous dependence of the diffusion coefficient on the parallel velocity, which follows from the non-monotonous dependence of the spectra of parallel electric fields on the KAW perpendicular wavenumber.

3.1. Fokker-Planck Diffusion Coefficient in Terms of KAWs' Magnetic Fields

Since the parallel electric fields $E_{z\mathbf{k}}$ in KAWs are relatively weak and difficult to measure, it is instructive to express D^A in terms of KAWs' magnetic fields. To this end one can use the KAW polarization relation

$$\frac{E_z}{B_\perp} = -\frac{T_{ez}}{T_{p\perp}} \frac{V_A}{c} \frac{k_z}{k_\perp} \frac{\mu^2}{K}. \quad (11)$$

Then the 2D velocity-space diffusion coefficient for the protons can be reduced to the following integral in the normalized wavenumber space:

$$\begin{aligned} D^A &= \pi^2 \frac{T_{ez}}{T_{p\perp}} \Omega_p V_S^2 \int d\mu \delta(\mu - K^{-1}) \frac{\mu^3 J_0^2}{K^2 \partial K / \partial \mu} \frac{\int d\nu \nu |B_{\mu\nu}|^2}{B_0^2} \\ &= \pi^2 \frac{T_{ez}}{T_{p\perp}} \Omega_p V_S^2 \left[\frac{\mu^3 J_0^2}{K^2 \partial K / \partial \mu} \frac{\int d\nu \nu |B_{\mu\nu}|^2}{B_0^2} \right]_{\mu=K^{-1}}. \end{aligned} \quad (12)$$

The dimensionless parallel wavenumber $\nu = \delta_p k_z$ (δ_p is the ion inertial length) is introduced in Equation (12), and the following relation for the Dirac δ -function is used:

$$\delta(K - V_z/V_A) = \frac{\delta(\mu - K^{-1})}{\partial K / \partial \mu},$$

where $K^{-1} = K^{-1}(V_z/V_A)$ is the inverse K -function of V_z/V_A and $V_S = \sqrt{T_{ez}/m_p}$ is the ion-sound speed. The normalized spectral density, $|B_{\mu\nu}|^2 = \delta_p^{-1} \rho_p^{-2} |B_{\perp\mathbf{k}}|^2$, is defined such that $\int dk_z \int dk_\perp k_\perp |B_{\perp\mathbf{k}}|^2 = \int d\nu \int d\mu \mu |B_{\mu\nu}|^2$. Note that $|B_{\mu\nu}|^2$ has the same dimension as B_0^2 .

Now we have to express the integral $\int_0^\infty d\nu \nu |B_{\mu\nu}|^2$ in terms of the integral power at μ , $|B_\mu|^2 = \int d\nu |B_{\mu\nu}|^2$. This last quantity is related to the unidirectional spectral density W_μ measured by spacecraft: $\mu |B_\mu|^2 = W_\mu$. The perpendicular wavenumber μ is related to the measured spacecraft-frame frequency f through $\mu \sin \theta_{VB} \simeq (V_{Tp}/V_{SW}) (f/f_p)$, θ_{VB} is the angle between the solar wind velocity V_{SW} and B_0 .

In principle, an unknown spectrum of parallel wavenumbers ν contributes to the turbulence level at every particular μ . To simplify the problem, we take into account the following two facts. First, theory and observations suggest that the turbulence cascade proceeds along a path in wavenumber space which is defined by the "critical balance" between the linear and nonlinear time scales (Goldreich and Sridhar, 1995). In accordance to the critical balance condition, every particular μ has its own ν_μ where most of the spectral density is concentrated: $|B_{\mu\nu}|^2 = |B_\mu|^2 \delta(\nu - \nu_\mu)$, where $|B_\mu|^2$ is the turbulence level at the perpendicular wavenumber μ . Second, the turbulence fluctuations are anisotropic with $k_\perp \gg k_z$. Denoting the anisotropy factor $k_z/k_\perp \equiv \alpha(k_\perp)$, the critical balance reads $\nu_\mu = \frac{V_A}{V_{Tp}} \alpha(\mu) \mu$. Hence we estimate $\int_0^\infty d\nu \nu |B_{\mu\nu}|^2 \simeq \frac{V_A}{V_{Tp}} \alpha(\mu) \mu |B_\mu|^2 = \frac{V_A}{V_{Tp}} \alpha(\mu) W_\mu$, and

$$D^A = \pi^2 \left(\frac{T_{ez}}{T_{p\perp}} \right)^{3/2} \Omega_p V_S V_A \left[\frac{\alpha(\mu) \mu^3 J_0^2 W_\mu}{K^2 \partial K / \partial \mu B_0^2} \right]_{\mu=\mu_v}, \quad (13)$$

where $\mu_v = K^{-1}(V_z/V_A)$.

3.2. Diffusion Coefficient for Double-kink Power-law Turbulence Spectra

Further progress is possible if we know a particular shape of the turbulent spectrum of the Alfvénic turbulence. Numerous in-situ observations indicate that the power law spectra $W_\mu \propto \mu^{-p}$ are typical in the solar wind, but the spectral index p is different in different ranges of μ . In the MHD turbulence range $\mu \leq \mu_1$ the power law index $p = p_1 \simeq 1.7$, close to the Kolmogorov value. In the intermediate weakly/mildly dispersive KAW range $\mu_1 \leq \mu \leq 1$ the spectra are much steeper, with $p = p_2$ varying from $p_2 = 2$ to $p_2 = 4$ (Leamon *et al.* 1999; Smith *et al.* 2011; Sahraoui *et al.*, 2010). In the strongly dispersive KAW range, $\mu \gg 1$, the power index approaches the value $p = p_3 \simeq 2.8$ (Alexandrova *et al.*, 2009; Sahraoui *et al.*, 2010). All the above double-kink behavior of $p(\mu_v)$ can be modeled by the following piecewise function:

$$p = p(\mu) = p_1 + (p_2 - p_1) H(\mu - \mu_1) + (p_3 - p_2) H(\mu - \mu_2), \quad (14)$$

where $H(x)$ is the Heaviside step function, $H(x) = 0$ for $x < 0$ and $H(x) = 1$ for $x \geq 0$. The spectral break (more precisely, the first spectral kink) at $\mu_1 = 0.1-0.5$ separates MHD and (weakly/ dispersive) kinetic ranges of Alfvénic turbulence. The second spectral kink, that occurs at $\mu_2 = 2-3$ (see spectra measured by Sahraoui *et al.* (2010), separates weakly and strongly dispersive KAW ranges (Voitenko and De Keyser, 2011).

With Equation (14), the measured spectral density can be written in the following general form:

$$W_\mu = W_{\mu_1} \left(\frac{\mu_2}{\mu_1} \right)^{(p_3-p_2)H(\mu-\mu_2)} \left(\frac{\mu}{\mu_1} \right)^{-(p_1+(p_2-p_1)H(\mu-\mu_1)+(p_3-p_2)H(\mu-\mu_2))}, \quad (15)$$

where W_{μ_1} is the turbulence spectral density at $\mu = \mu_1$ (note that W_{μ_1} has dimension of B_0^2). The re-normalization of the spectrum (Equation (15)) at $\mu \geq \mu_2$ ensures it is continuous through the second kink at $\mu = \mu_2$.

With Equation (15) the velocity diffusion coefficient (Equation (13)) attains the following general form:

$$D^A = \pi^2 \Omega_p V_S V_A \frac{\left(\frac{T_{ez}}{T_{p\perp}}\right)^{3/2}}{\left(1 + \frac{T_{ez}}{T_{p\perp}}\right)} \times \frac{\mu_1^2 \alpha(\mu_v) \left(\frac{\mu_2}{\mu_1}\right)^{(p_3-p_2)H(\mu_v-\mu_2)} \left(\frac{\mu_v}{\mu_1}\right)^{2-p(\mu_v)} J_0^2\left(\mu_v \frac{V_{\perp}}{V_{Tp}}\right) W_{\mu_1}}{\frac{V_z}{V_A} B_0^2}, \quad (16)$$

where $\mu_v = \mu(V_k = V_{\parallel})$ is the resonant KAW wavenumber defined by Equation (7) and $p(\mu_v)$ is given by Equation (14). In what follows we will put $\alpha(\mu) \simeq 0.1$ at ion kinetic scales $\mu \approx 1$ (Sahraoui *et al.*, 2010), and neglect its relatively slow variation in the resonant wavenumber range.

The diffusion due to KAWs is strongest for the protons with velocities around $V_z \simeq V_1 \gtrsim V_A$, which are Cherenkov-resonant with the spectral peak of the KAW parallel electric fields. In the plane $\perp B_0$, the diffusion is maximized for the core protons at $V_{\perp} \lesssim V_{Tp}$, where the reduction due to proton-cyclotron gyration is minimized. In the B_0 -parallel direction, the diffusion coefficient decreases very fast as $V_z \rightarrow V_A$, and less fast with V_z growing in a more extended velocity range from V_1 to several Alfvén velocities. These features are compatible with the physical picture of the Cherenkov resonant interaction between gyrating particles and waves with finite cross- B_0 length scales.

Since there are no positive $\mu = K^{-1}(V_z/V_A)$ for $V_z/V_A < 1$, $D^A = 0$ there (this fact reflects the absence of resonant KAWs for particles moving with sub-Alfvénic velocities $V_z/V_A < 1$). One should note, however, that even sub-Alfvénic protons can be affected by the turbulence fluctuations via two effects: (i) nonlinear broadening of the Cherenkov resonances, and (ii) increased Coulomb diffusion of the protons at the steep VDF slope at $V_z \lesssim V_A$. The minimum velocity of the affected protons resulting from the former effect is analytically estimated below in Equation (22).

It is interesting to note that the spectral slope $p(\mu_v) < 2$ in (14) can make D^A a still increasing function of μ_v in the dissipation range between μ_1 and μ_2 . This follows from the increase of the parallel electric fields in KAWs that is faster than the power-law decrease of the turbulence amplitudes. Therefore, depending on $p(\mu_v) \lesssim 2$, the diffusion coefficient attains a maximum value at $\mu_v = \mu_1$ (with $p(\mu_v) > 2$) or at $\mu_v \lesssim \mu_2$ (with $p(\mu_v) < 2$). Such behavior of the diffusion coefficient could have an important consequence that the less steep dissipation-range spectra result in longer nonthermal tails in the proton VDFs. However this could only be true for the cases where the turbulence amplitude is the same at $\mu = \mu_1$.

In fact, as was found by Smith *et al.* (2006) in the inertial range, the larger spectral fluxes ϵ are followed by the steeper dissipation-range spectra p_2 , such

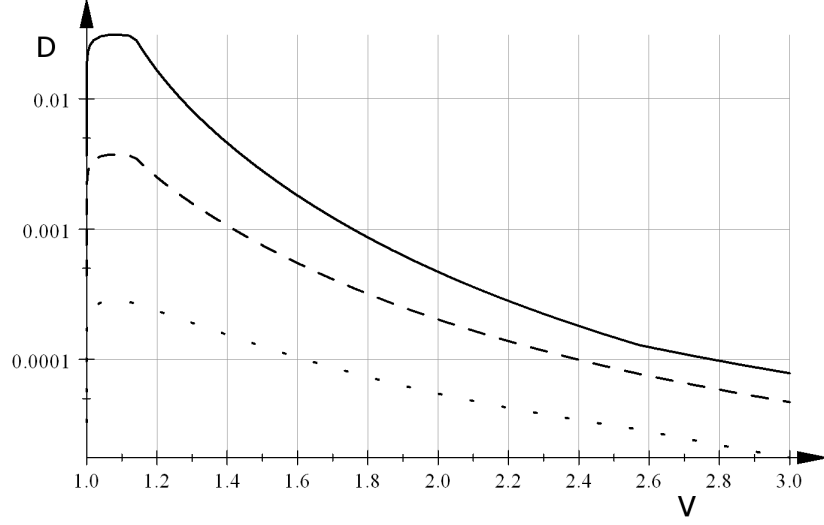


Figure 2. Reduced diffusion coefficient as function of normalized parallel velocity $V = V_z/V_A$ for $p_2 = 2$ (dot line), $p_2 = 3$ (dash line), and $p_2 = 4$ (solid line). Turbulence level at the first spectral kink is adjusted for each p_2 using the scaling $W_{\mu 1} \propto p^{7.4}$.

that $p_2 = 1.05\epsilon^{0.09}$. Applying this relation at the end of inertial range, we find the scaling

$$W_{\mu 1} \propto p_2^{7.4}, \quad (17)$$

relating the spectral power $W_{\mu 1}$ at the break $\mu = \mu_1$ and the spectral index p_2 above it. If the spectral powers in two cases (1) and (2) are $W_{\mu 1}^{(1)}$ and $W_{\mu 1}^{(2)}$, then the ratio $W_{\mu 1}^{(1)}/W_{\mu 1}^{(2)} = (p_2^{(1)}/p_2^{(2)})^{7.4}$. Elaborating this scaling relation, a reduced 1D diffusion coefficient is shown in Figure 2 for three spectral indices $p_2 = 4, 3$, and 2 from top to bottom. The reduction was performed by the averaging of J_0^2 in (16) in the cross-field velocity plane. With the correlation found by Smith *et al.* (2006), the diffusion coefficient, in average, is larger for steeper dissipation-range spectra, even if they decrease with V_z faster.

The described above properties of the diffusion coefficient indicate that kinetic Alfvén turbulence can be efficient in diffusing the protons in the velocity range covered by nonthermal tails of the proton VDFs. This is supported by the analytical and numerical estimations presented below.

4. Evolution of Nonthermal Tails in the Proton VDFs

We investigate here what nonthermal proton tails can be formed by their quasi-linear diffusion along the kinetic turbulent spectrum described above. Let us consider a local evolution problem in the solar wind neglecting external forces,

spatial variations, and Coulomb collisions in Equation (9). To estimate the formation time for a particular tail, we have to know the tail extension in the field-aligned direction V_{\max} . Observations show that the tail extension V_{\max} rarely exceeds $3V_A$, which allows us to simplify the problem accounting only for the intermediate KAW spectrum in the diffusion coefficient (Equation (16)). The cross-field velocity spread in the tails is approximately the same as in the proton core, $\approx V_{T_{p\perp}}$ (within the multiplier of the order 1).

Accounting for above, we reduce Equation (9) to the 1D diffusion equation

$$\frac{\partial f}{\partial t} = \frac{\partial}{\partial V_z} D \frac{\partial f}{\partial V_z} \quad (18)$$

for the reduced 1D distribution function $f = f(V_z) = 2\pi \int dV_\perp V_\perp F(V_z, V_\perp)$. The 1D diffusion coefficient in the range $V_A < V_z < 3V_A$,

$$D \simeq 0.1\pi^2 \Omega_p V_S V_A \frac{(T_{ez}/T_{p\perp})^{3/2}}{(1 + T_{ez}/T_{p\perp})} \frac{\mu_1^{p_2} \Lambda_0 (\mu_v^2)}{\mu_v^{p_2-2}} \frac{V_A}{V_z} \frac{W_{\mu_1}}{B_0^2}, \quad (19)$$

follows from Equation (16) after averaging over Maxwellian distribution in the cross-field plane: $\langle J_0^2 \left(\mu_v \frac{V_\perp}{V_{Tp}} \right) \rangle = \Lambda_0 (\mu_v^2)$.

For small μ_1 the corresponding resonant velocity $V_1 = V_A K(\mu_1)$ is close to V_A and the remaining velocity interval $V_A < V_z < V_1$ is narrow. The detailed behavior of the diffusion coefficient D is unimportant there because D decreases fast to 0 with $V_z \rightarrow V_A$, and the nonlinear resonance broadening of KAWs with $\mu \simeq \mu_1$ is more important.

4.1. Quasilinear Plateau Model

In this section we study the quasilinear plateau evolution under the influence of the KAW turbulence. To this end we start from the initially isotropic Maxwellian VDF for the protons

$$f_{t=0} = f_M = \frac{1}{\sqrt{2\pi} V_{Tp\parallel}} \exp \left(-\frac{V_z^2}{2V_{Tp\parallel}^2} \right).$$

The diffusion coefficient (Equation (19)) and hence the velocity-space diffusion are very non-uniform, as is seen from Figure 2. The diffusion is fastest in the vicinity of V_A , where the diffusion coefficient is maximal, but decreases about two orders at $3V_A$. The quasilinear saturation in this situation occurs first around this maximum, where an initial local plateau is formed as is shown in Figure 3 (dashed line). The resulting 1D proton VDF can be modeled by the piece-wise function with the local plateau

$$f = f_{pl} = \frac{\bar{n}_{pl}}{V_{\max} - V_{\min}} \quad (20)$$

in the velocity range $V_{\min} < V_z < V_{\max}$, and f remaining Maxwellian, $f = f_M$, outside the plateau.

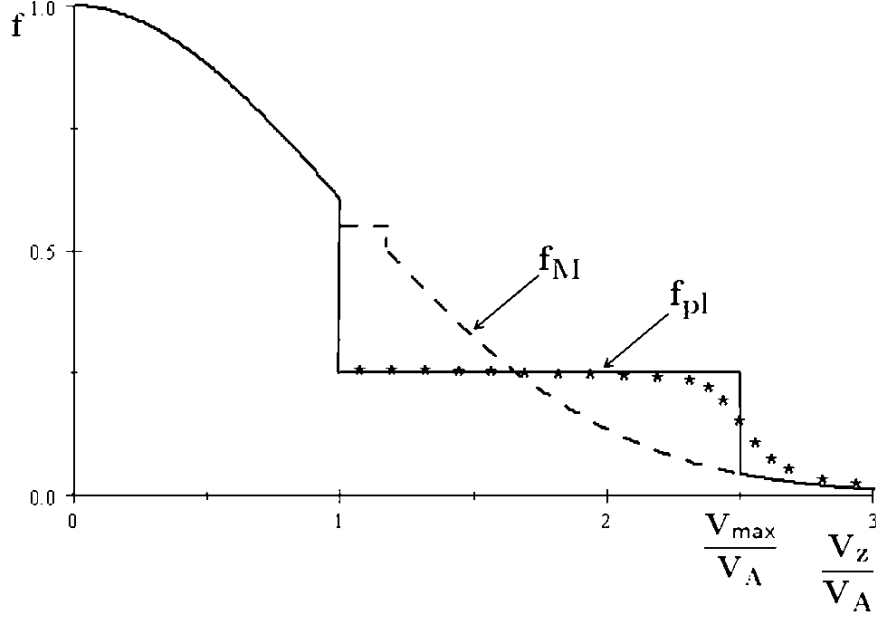


Figure 3. Model proton VDF with a step-like quasilinear plateau extending to $V_{\max} = 2.5V_A$ at the late evolutionary stage (an early evolutionary stage is shown by dash line). Numerical solution of the diffusion equation (Equation (18)) for the same time is shown by stars. A good correspondence is observed between the model and numerically calculated VDFs. Details on the plasma and turbulence parameters used are given in the text.

The quasilinear saturation spreads in time to higher velocities, shifting the plateau front $V_{\max} = V_{\max}(t)$ forward to higher velocities as is also shown in Figure 3 (solid line). The normalized proton number density in the plateau can be expressed in terms of error function Erf:

$$\bar{n}_{\text{pl}} = \frac{n_{\text{pl}}}{n_0} = \int_{V_{\min}}^{V_{\max}} dV_z f_M = \frac{\text{Erf}\left(\frac{V_{\max}}{\sqrt{2}V_{T_p}}\right) - \text{Erf}\left(\frac{V_{\min}}{\sqrt{2}V_{T_p}}\right)}{2}. \quad (21)$$

It increases with time, but the plateau height decreases.

It is important to note that the minimum velocity of the protons involved in the plateau formation, V_{\min} , can be less than the minimum phase velocity of resonant KAWs, V_A . As follows from the nonlinear broadening of the Cherenkov resonance for a KAW with wavenumber k_{\perp} and amplitude B_k , the minimum velocity of the affected protons is

$$\frac{V_{\min}}{V_A} = \sqrt{1 + k_{\perp}^2 \rho_T^2} - \sqrt{4 \frac{V_{p\parallel}}{V_A} \frac{T_{e\parallel}/T_{p\parallel}}{\sqrt{T_{p\perp}/T_{p\parallel}} + T_{e\parallel}/T_{p\parallel}}} \sqrt{\frac{k_{\perp} \rho_T}{\sqrt{1 + k_{\perp}^2 \rho_T^2}} \frac{B_k}{B_0}}. \quad (22)$$

This formula follows from the condition that the proton kinetic energy in the wave frame is equal to the KAW potential barrier. For $T_{e\parallel}/T_{p\parallel} = T_{p\perp}/T_{p\parallel} = 1$,

and the typical KAW amplitude $B_k/B_0 = 0.05$ in the vicinity of the first spectral break, at $k_\perp \rho_T = \sqrt{1 + T_{e\parallel}/T_{p\perp}} k_\perp \rho_p \simeq 0.3$, the minimum velocity reduces to $V_{\min} \simeq 0.8V_A$. The modified $V_{\min} < V_A$ can significantly increase the proton number density in the tail, and hence the energy in the parallel degree of freedom in comparison to the case $V_{\min} = V_A$. On the other hand, such decrease of V_{\min} does not influence much the evolution time scales of the tails.

4.2. Evolution Time Scale of the Quasilinear Plateau

The time evolution of the plateau spreading can be found from the diffusion equation (Equation (18)) as follows. First, we note that the time derivative of f_{pl} can be expressed as

$$\frac{\partial f_{pl}}{\partial t} = -\frac{f_{pl} - f_M(V_{\max})}{V_{\max} - V_{\min}} \frac{\partial V_{\max}}{\partial t}. \quad (23)$$

Using expression (23) in the lhs of the diffusion equation (Equation (18)) and then integrating it over the plateau velocity range, from $V_{\min} + 0$ to $V_{\max} + 0$, we obtain a first-order ordinary differential equation for V_{\max} as function of time t :

$$(f_{pl} - f_M(V_{\max})) \frac{dV_{\max}}{dt} = D(V_{\max}) \frac{\partial f_M(V_{\max})}{\partial V_{\max}}.$$

This equation can be solved easily by separating variables and integrating from $t = 0$ to t :

$$t = V_{Tp\parallel}^2 \int_{V_{\min}}^{V_{\max}} \frac{f_{pl}(V'_{\max})/f_M(V'_{\max}) - 1}{V'_{\max} D(V'_{\max})} dV'_{\max}. \quad (24)$$

Let us estimate the plateau formation time at 1 AU, where $\Omega_p \simeq 1 \text{ s}^{-1}$, $T_{ez}/T_{p\perp} \simeq T_{ez}/T_{pz} \simeq 1$ and $V_A \simeq V_{Tp} \simeq 50 \text{ km s}^{-1}$. With the turbulence amplitude $|B_1|/B_0 \simeq 0.05$, spectral break wavenumber $\mu_1 \simeq 0.6$, and spectral slope $p_2 = 3$ just above the break, (24) gives the time about half an hour for formation of quasilinear plateau with the length equal to the average tail length $V_{\max} = 1.75V_A$. Since this time is much (more than 2 orders) shorter than the solar wind expansion time t_{SW} (2-4 days at 1 AU), such tails can be easily generated by the turbulence locally in the solar wind.

A long tail with V_{\max} reaching $2.5V_A$ is developed by the $p_2 = 2$ turbulence at $t = 14 \text{ h}$, when the local approximation is still marginally applicable. The corresponding model solution is shown in Figure 3 by the solid line. Furthermore, to verify the model, we solve numerically the proton diffusion equation (Equation (18)) with the zero-gradient Neumann boundary conditions at the lower ($V_z/V_A = 1$) and upper ($V_z/V_A = 5$) boundaries. The value for the upper boundary is chosen in such a way that its variations does not affect solution in the velocity range $V_z/V_A = 1 - 3$. This solution is also shown in Figure 3 by stars. A good correspondence between numerical and analytical solutions indicates that the model (Equations (20)–(24)) is sufficient for quantitative estimations of the quasilinear plateau height, length, and evolution time-scale.

For longest tails with $V_{\max} \simeq 3V_A$, the tail formation time approaches the solar wind expansion time $t_{\text{SW}} = 2 - 4$ days. This means that the local analysis for such tails is inapplicable, but does not mean that such tails cannot be formed by the turbulence. To study such tails one needs to solve a nonlocal problem incorporating radial dependencies of the solar wind plasma and turbulence characteristics (this work is in progress). Again, even for such long tails as $V_{\max} \simeq 3V_A$, the problem can be made local with slightly increased turbulence amplitudes and/or spectral break wavenumbers, say to $|B_1|/B_0 \simeq 0.07$ and $\mu_1 \simeq 0.8$. Such variations are within the ranges of measured values (see Figure 2 by Markovskii, Vasquez, and Smith (2008)). In addition, as we will see below, the decrease of the spectral slope p_2 (with fixed amplitude B_1) has the same effect.

Since the plateau formation time given by Equation (24) is quite complex function of plasma and turbulence parameters, its radial dependence require further investigations using particular plasma and turbulence models. For example, with approximately constant break frequency (constant $k_{\perp 1}$), the plateau formation time decreases with decreasing R as, roughly, $\sim V_A \sim R$, the same as t_{SW} . In this case the locality condition can be still satisfied much closer to the Sun, where V_A is larger and hence longer tails can be generated. Several numerical estimations with reasonable plasma and turbulence parameters have shown that the tails $V_{\max} \approx 2V_A$ can be easily generated, within half an hour, at such short heliocentric distances as $R \approx 0.1$ AU, where $t_{\text{SW}} \approx 5 - 7$ h. The conditions are even more favorable with constant μ_1 . These estimations are compatible with Helios observations of nonthermal proton tails at all distances from 0.3 to 1 AU.

Figure 4 shows the time evolution of the plateau boundary $V_{\max} = V_{\max}(t)$ in a turbulence with the spectral power $W_{f_1} \simeq 0.2 \text{ nT}^2 \text{ Hz}^{-1}$ at the break frequency $f_1 \simeq 0.3$ Hz. These values are well within ranges of measured values and close to the average ones (see Figures 1 and 2 by Markovskii, Vasquez, and Smith (2008)). Five curves in Figure 4 correspond to five different spectral slopes $p_2 = 2, 2.5, 3, 3.5$, and 4 (from top to bottom). Longer dashes indicate larger p_2 , except for the solid curve with $p_2 = 3$. It is seen that the formation time $t = t_{\text{QL}}$ for the plateau $V_{\max} = (1.5 - 2.5)V_A$ is considerably shorter than the solar wind expansion time, $t_{\text{QL}}/t_{\text{SW}} = 0.01 - 0.3$ (we assume an average $t_{\text{SW}} = 2.7 \times 10^5$ s). With these values, covering typical proton nonthermal tails observed in the solar wind, the quasilinear diffusion process can be considered in the local approximation and our results are self-consistent. As the tail length approaches $3V_A$, the corresponding evolution time scale approaches t_{SW} for the shallowest spectra. This suggests that in average plasma conditions the tail length can hardly exceed $3V_A$, except for the cases of high turbulence levels combined with shallow spectra.

In Figure 5 we are looking for the favorable conditions facilitating local production of nonthermal proton tails in the solar wind. To this end we fix the plateau front at $V_{\max} = 1.5$ and plot the corresponding formation time as function of V_{Tp}/V_A (which is proportional to the square root of the proton plasma beta). The spectral indexes are $p_2 = 2.5, 3, 3.5$, and 4 for the four curves from bottom to top. The most favorable V_{Tp}/V_A for each curve is that one at which t/t_{SW} attains minimum. The shallowest spectra appeared to be most

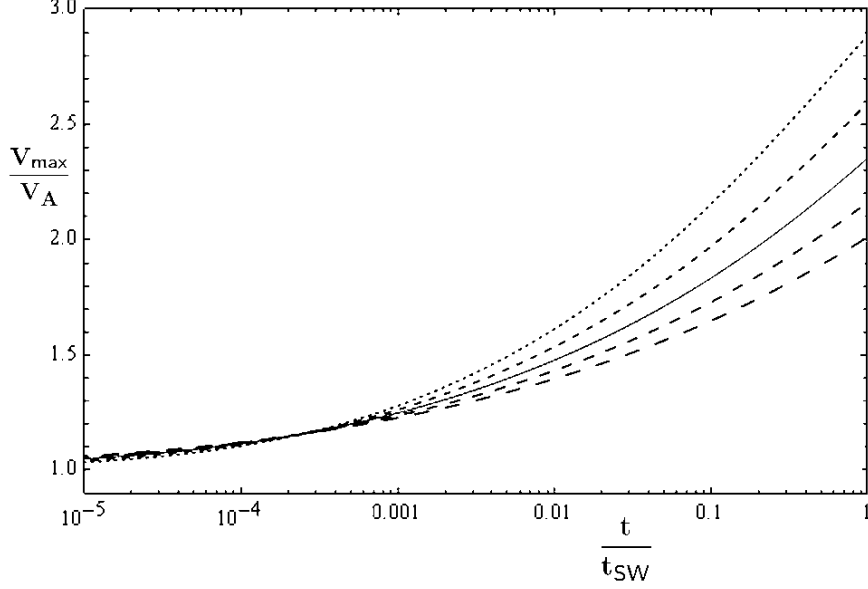


Figure 4. Normalized tail length V_{\max}/V_A as function of normalized time t/t_{SW} . Spectral slopes are $p_2 = 2, 2.5, 3, 3.5$, and 4 from the top curve to bottom. All other plasma and turbulence parameters are the same for all curves (see text).

efficient at $V_{\text{Tp}}/V_A \simeq 1.5$, whereas the steepest spectra at $V_{\text{Tp}}/V_A \lesssim 1$. These values are not much different for all spectral slopes of interest, so that we can take the optimal value $V_{\text{Tp}}/V_A \approx 1$, which is close to the average value in the solar wind at 1 AU. This means that the turbulence at 1 AU become more efficient in producing nonthermal tails.

In general, as is seen from Figures 4 and 5, the shallower kinetic spectra are more efficient in the tail production provided all other turbulence characteristics are fixed. However, not only the spectral slope, but also the level of turbulence is highly variable in the solar wind. Moreover, as was noticed by Smith *et al.* (2006), there is a positive correlation between the spectral flux before the spectral break and the spectral slope after it. The corresponding scaling in terms of spectral power can be written as $W_{\mu 1} \propto p_2^{7.4}$. Rescaling the turbulence amplitudes corresponding to $p_2 = 2, 2.5, 3.5$, and 4 slopes, we plot the resulting plateau front velocities for each p_2 in Figure 6. Now we obtain an opposite ordering of V_{\max} with p_2 , indicating that longer tails are generated by steeper spectra. Another new feature is less scattered final values of V_{\max} as compared to the case of uncorrelated amplitudes and slopes.

4.3. Numerical Example

At present, there are no data on the proton VDF and kinetic-scale turbulence measured simultaneously. The problem with the Cluster spacecraft is that they

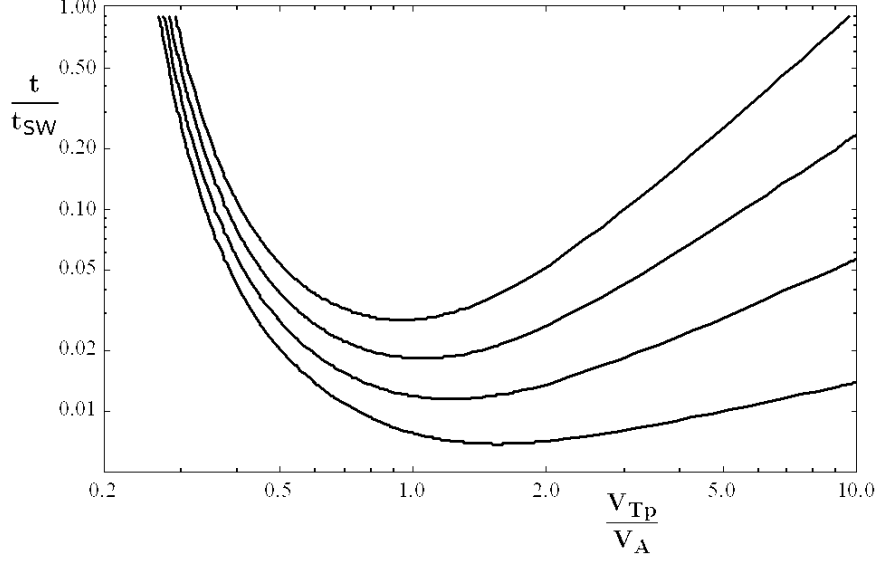


Figure 5. Formation time of the tail with $V_{\max} = 1.5V_A$ as function of the proton thermal/Alfvén velocity ratio V_{Tp}/V_A for the spectral slopes $p_2 = 2.5, 3, 3.5$, and 4 (from top to bottom). Other parameters are as in Figures 3 and 4.

are capable of measuring the turbulence at sufficient frequency resolution, but the proton velocity-space resolution is insufficient in the solar wind conditions. It is nevertheless interesting to estimate a nonthermal proton tail that could result from a turbulence measured by Cluster.

In a particular case of Cluster measurements 10 January 2004 from 06:15 to 06:25 UT, reported by Sahraoui *et al.* (2010), the background plasma parameters are: $B_0 = 10.2$ nT, $n_0 = 16$ cm $^{-3}$, $T_e = 10.4$ eV, $T_p = 31$ eV, $V_{SW} = 548$ km s $^{-1}$, angle between the solar wind velocity and magnetic field $\theta_{BV} = 67^\circ$. Therefore, the proton thermal velocity in this case is about the same as the Alfvén velocity, $V_{Tp} \simeq V_A \simeq 55$ km s $^{-1}$, proton cyclotron frequency $\Omega_p \simeq 0.94$ s $^{-1}$, proton gyroradius $\rho_p \simeq 59$ km, and solar wind expansion time $t_{SW} = 76$ hours. The key turbulence characteristics are: spectral index at the proton kinetic scales $p = p_2 = 4$, spectral break $\mu_1 = 0.4$, and the turbulence spectral density $W_{\mu 1} \simeq 0.15$ nT 2 at $\mu = \mu_1$.

The dependence $V_{\max}(t)$ for this case is given by the bottom line in Figure 4. One can observe that the turbulence should generate a nonthermal proton tail with $V_{\max} \lesssim 2V_A$ at 1 AU. The proton VDF could not be measured by Cluster, but the average parallel energy of the protons was found to be larger than the perpendicular one, producing the effective temperature anisotropy $T_{p\parallel}/T_{p\perp} \lesssim 1.5$. This anisotropy cannot be produced by the quasilinear evolution of the initially isotropic Maxwellian VDF in the velocity range from V_A to $2V_A$. To

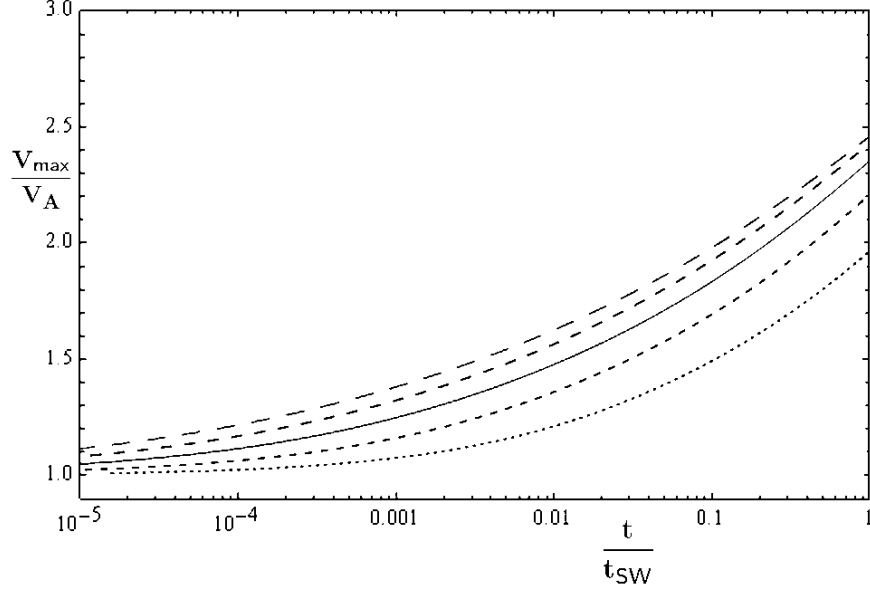


Figure 6. Normalized tail length V_{\max}/V_A as function of normalized time t/t_{SW} for the same parameters as in Figure 4 except for the turbulence amplitudes are now adjusted by the scaling $W_{\mu 1} \propto p_2^{7.4}$. In this case the order of curves is reversed, $p_2 = 2, 2.5, 3, 3.5$, and 4 from bottom to top, which means the longer tails are generated by steeper spectra.

obtain such anisotropy, one needs either more protons in the tail, or longer tail ($V_{\max} > 2V_A$), or both. The additional protons can be delivered to the tail by the nonlinear broadening of the Cherenkov resonance at $\mu \simeq \mu_1$, as is given by Equation (22), and/or by the enhanced collisional diffusion at the steep velocity-space gradients at $V_z \simeq V_{\min}$, where VDF undergoes a sharp transition from the Maxwellian VDF to the plateau-like. Most probably, both these processes have non-negligible effects on the tail density, and act synergetically. Again, we would like to stress that the tail length is not much affected by these processes. The longer tail could only be generated at shorter radial distances to the Sun, in more favorable conditions.

5. Conclusions and Discussion

We studied a Fokker-Planck proton diffusion in the solar wind induced by Alfvénic turbulence observed recently at proton kinetic scales (Sahraoui *et al.*, 2010; He *et al.*, 2011, 2012; Podesta and Gary, 2011; Salem *et al.*, 2012). Observations indicate that the turbulence is anisotropic and dominated by large perpendicular wavevectors, which is typical for KAWs possessing parallel electric fields and hence experiencing Cherenkov resonances. In the presence of a wide

KAW spectrum with overlapping harmonics, the protons undergo numerous Cherenkov kicks resulting in a Fokker-Planck proton diffusion in the velocity space along the mean magnetic field.

We derived a quasilinear diffusion equation with the diffusion coefficient expressed in terms of measured turbulence parameters: spectral break wavenumber μ_1 , turbulence amplitude W_{μ_1} at the spectral break, and spectral slopes p_2 below the break. At small and large μ , the asymptotic values for the spectral index are $p \simeq 1.7$ and 2.7 , respectively (*e.g.* Alexandrova *et al.*, 2009). There is however an intermediate spectral range, $\mu_1 < \mu < \mu_2$, where the spectrum slope is variable and often steepens to $p \simeq 3-4$ or even higher values (Sahraoui *et al.*, 2010). The turbulence power at these scales is mostly in form of weakly/mildly dispersive KAWs that are Cherenkov-resonant with protons in the velocity range covered by observed nonthermal tails, $V_z \simeq (1-3) V_A$. Enhanced nonlinear interaction among KAWs can explain such steep spectra in this range (Voitenko and De Keyser, 2011), but resonant generation of nonthermal tails can contribute to the steepening as well. On the other hand, an additional source for the KAW replenishing in the dissipation range can be provided by the non-local nonlinear coupling among KAWs and large-scale MHD AWs (Zhao, Wu, and Lu, 2011).

Rudakov *et al.* (2012) applied an asymptotic analysis to study the quasilinear proton diffusion in the strongly dispersive KAW turbulence with $\mu \gg 1$, which implies relatively high-energy resonant protons with $V_z \gg V_A$. However, such asymptotical analysis is inapplicable to typical tails with proton velocities $V_A < V_z < 3V_A$. The reason is that the KAW phase velocity (Equation (6)) cannot be approximated by a simple power-law dependence in the resonant wavenumber range $0.3 < \mu < 3$. We focused on this tail-resonant range, where most of kinetic-scale power is residing and where the full KAW dispersion (Equation (6)) has to be used. Consequently, the resulting diffusion equation is more complex and does not have an immediate analytical solution similar to that found by Rudakov *et al.* (2012). To proceed further analytically, we took into account a fast decrease of the diffusion coefficient with growing V_z (see Figure 2), which allowed us to formulate a simple yet plausible model for the quasilinear plateau, Equations (21) and (21), with the time-dependent front velocity V_{\max} and height f_{pl} . By the use of this model in the diffusion equation (Equations (18) and (19)), we found an analytical solution (Equation (24)) for the plateau formation time as function of the plateau front velocity V_{\max} . Several numerical tests (one of them is shown in Figure 3) have confirmed the applicability of this model in the solar wind conditions.

In general, our analysis and numerical estimations have revealed that the quasilinear proton diffusion driven by the observed solar wind turbulence provides a robust generation mechanism for nonthermal proton tails, which can explain their routine observations in the solar wind. By implementing the measured characteristics of the turbulence at proton kinetic scales μ_1 , W_{μ_1} , and p_2 in our model, we estimated the time scale of the quasilinear plateau formation in the velocity space. For typical nonthermal tails with $V_{\max} = (1.5 - 2.5) V_A$ the estimated formation time is $0.5 - 3$ h, which is much less than the solar wind expansion time at 1 AU. This indicates that the local generation of such tails observed in the solar wind is a natural consequence of the observed kinetic-scale Alfvén turbulence.

Some longer tails may require more time to develop, in which case a non-local radially-dependent problem has to be solved numerically using suitable solar wind models. In principle, with sufficient KAW power at $\mu > \mu_2$, the quasilinear plateau can extend well above $3V_A$, where an asymptotic $\mu \gg 1$ analysis by Rudakov *et al.* (2012) is applicable. However, the turbulence level is usually insufficient to form the tails with $V_{\max} > 3V_A$ within required time scales, which is reflected in the fast growth of the formation time beyond t_{SW} . This constrain is compatible with rare observations of such long tails.

The most favorable conditions for the tail generation in terms of V_{Tp}/V_A occur in the range $V_{\text{Tp}}/V_A \simeq 1 - 1.5$ for spectral slopes ranging from $p_2 = 2.5$ to 4, correspondingly. The optimal $(V_{\text{Tp}}/V_A)_{\text{opt}}$ is not much varying with the spectral slopes in the range of interest, and we can say that in general $(V_{\text{Tp}}/V_A)_{\text{opt}} \approx 1$. Such conditions are often met at 1 AU. As is seen from Figure 5, the range of V_{Tp}/V_A allowing for the tail generation has two bounds, upper $(V_{\text{Tp}}/V_A)_{\text{cr2}}$ and lower $(V_{\text{Tp}}/V_A)_{\text{cr1}}$. The upper bound $(V_{\text{Tp}}/V_A)_{\text{cr2}}$ is relatively large, its values for different spectral slopes are very scattered, and it is not very restrictive for the tail generation. On the contrary, the lower bound $(V_{\text{Tp}}/V_A)_{\text{cr1}}$ is more restrictive. It has more collimated values that are not much different from each other and are not so small, which is seen from Figure 5. Say, for $V_{\max} \simeq 1.5V_A$ tails $(V_{\text{Tp}}/V_A)_{\text{cr1}} \simeq 0.25$ and such tails cannot be generated locally if $V_{\text{Tp}}/V_A < 0.25$. The range of favorable V_{Tp}/V_A can not be extended towards smaller values. It seems that only short tails with $V_{\max} < 1.5V_A$ can be generated at $V_{\text{Tp}}/V_A \approx 0.1$. Relatively long tails are expected with steep spectral slopes p_2 that are positively correlated with turbulence levels.

We also analyzed a particular case reported by Sahraoui *et al.* (2010). We found that the measured turbulence can generate a nonthermal tail extending to $V_{\max} \lesssim 2V_A$, but the proton number density in the tail is insufficient to explain the measured temperature anisotropy of the protons. We suggest that the nonlinear resonance broadening and enhanced collisional diffusion at $V_z \lesssim V_A$ are important mechanisms significantly increasing the proton number density in the tail. Yet another possibility is that the longer tail producing larger measured anisotropy was generated at shorter radial distances. The related effects require further investigation.

Behind the amplitude-related constraints mentioned above, the tail length and shape can also be constrained by plasma instabilities. Several instabilities can develop on the plateau-like proton tail, including the fast magnetosonic, parallel Alfvén-cyclotron (Rudakov *et al.*, 2012), and oblique Alfvén (Daughton and Gary, 1999; Voitenko and Goossens, 2003) instabilities. Although Daughton and Gary (1999) and Voitenko and Goossens (2003) studied instability driven by the bump-on-tail, its generation mechanism is related to the anomalous Doppler (proton-cyclotron) resonance rather than the inverse Landau damping, and hence is not restricted to the bump-on-tail but can also be efficient with plateau-like distributions. The cyclotron diffusion of tail protons, driven by these instabilities, can constrain tail lengths and produce proton-cyclotron quasilinear plateau reported by Marsch and Tu (2001) and Marsch and Bourouaine (2011), or even produce the bump-on-tail features. In turn, the nonthermal proton tails and beams can re-emit KAWs (Daughton and Gary, 1999; Voitenko and Goossens, 2003; ■

Wu, Chen, and Wu, 2012; Nariyuki, Hada, and Tsubouchi, 2012) and significantly modify the nonlinear evolution of the high-amplitude circularly-polarised Alfvén waves (Nariyuki, Hada, and Tsubouchi, 2009, 2012). A complex interplay of these processes requires further investigations.

Obtained analytical expressions for the proton diffusion coefficient can be incorporated in more sophisticated solar wind models accounting for external forces (electric and gravity), and both the particle-particle (Coulomb) and the wave-particle (Cherenkov) interaction terms in the right-hand side of Equation (9). Because of their complexity, such models need to be solved numerically. Our preliminary simulation results demonstrate that the kinetic-scale Alfvénic turbulence can create such nonthermal tails in the proton VDFs at the radial distances $\lesssim 20$ solar radii (see detailed descriptions of these simulations in our accompanying paper (Pierrard and Voitenko, 2012)).

We did not concern here the bump-on-tail features (proton beams) often observed in the solar wind. Such distributions have not been reproduced by the uniform quasilinear diffusion we studied. However, with variable level of the turbulence launched through the solar wind base, the irregularity of the generated tail length can easily produce the bump-on-tail features by the time-of-flight effect. Namely, in a region of enhanced turbulence the high-velocity end of a dense nonthermal tail propagates faster than the bulk protons. As a consequence, at larger radial distances this proton population penetrates a more quiet region with a weaker tail and appears there as a bump on tail. This mechanism is compatible with Helios observations of time-variable bumps on virtually persistent tails (Marsch *et al.*, 1982).

In conclusion, appearance of nonthermal proton tails and beams in the solar wind is unavoidable in the presence of kinetic-scale Alfvénic turbulence with sufficient amplitude. There are several other generation mechanisms for proton beams and tails (see Introduction), which can compete with each other or replace in varying solar wind conditions. More detailed statistical correlation studies are needed to discriminate among them and to find what mechanism is dominant in the solar wind. It would be particularly interesting to have a look at correlations between the tail lengths and/or densities and the turbulence levels at kinetic scales.

Acknowledgements This research was supported by the Belgian Federal Science Policy Office (via IAP Programme, project P7/08 CHARM) and by the European Commission’s FP7 Program (projects 263340 SWIFF, and 313038 STORM). We thank the referee for his constructive criticism that helped us to improve this paper.

References

- Alexandrova, O., Saur, J., Lacombe, C., Mangeney, A., Mitchell, J., Schwartz, S. J., Robert, P.: 2009, *Phys. Rev. Lett.* **103**, 165003.
 Araneda, J. A. , Marsch, E., Vinas, A. F.: 2008, *Phys. Rev. Lett.* **100**, 125003.
 Borovsky, J. E. , Gary, S. P.: 2011, *J. Geophys. Res.* **116**, A07110.
 Chandran, B., Li, B., Rogers, B. N., Quataert, E., Germashevski, K.: 2010, *Astrophys. J.* **720**, 503.
 Cranmer, S., Matthaeus, W., Breech, B., Casper, J.: 2009, *Astrophys. J.* **702**, 1604.

- Daughton, W., Gary, S. P.: 1999, *Astrophys. J.* **602**, 1604.
- Galinsky, V. L., Shevchenko, V. I.: 2012, *Astrophys. J.* **602**, 1604.
- Gogoberidze, G., Chapman, S. C., Hnat, B.: 2012, *Phys. Plasmas* **19**, 102310.
- Goldreich, P., Sridhar, S.: 1995, *Astrophys. J.* **438**, 763.
- Hasegawa, A., Chen, L.: 1976, *Phys. Fluids* **19**, 1924.
- He, J., Marsch, E., Tu, C., Yao, S., Tian, H.: 2011, *Astrophys. J.* **731**, 85.
- He, J., Tu, C., Marsch, E., Yao, S.: 2012, *Astrophys. J. Lett.* **745**, L8.
- Hollweg, J. V., Isenberg, P. A.: 2002, *J. Geophys. Res.* **107**, 1147.
- Howes, G.: 2011, *Astrophys. J.* **738**, 40.
- Lamy, H., Pierrard, V., Maksimovic, M., Lemaire, J.: 2003, *J. Geophys. Res.* **108**, 1047.
- Li, X., Lu, Q., Chen, Y., Li, B., Xia, L.: 2010, *Astrophys. J. Lett.* **719**, L190.
- Lie-Svendsen, O., Leer, E.: 2000, *J. Geophys. Res.* **105**, 35.
- Markovskii, S. A., Vasquez, B. J., Smith, C. W.: 2008, *Astrophys. J.* **675**, 1576.
- Marsch, E.: 1991, In: Schwenn, R., Marsch, E. (eds.), *Physics of the Inner Heliosphere Vol. II*, Springer Verlag, Heidelberg, 45.
- Marsch, E.: 2006, *Living Rev. Solar Phys.* **3**(1), <http://solarphysics.livingreviews.org/Articles/lrsp-2006-1/> ■
- Marsch, E., Muehlhauser, K.-H., Schwenn, R., Rosenbauer, H., Pilipp, W., Neubauer, F.: 1982, *J. Geophys. Res.* **87**, 52.
- Marsch, E., Tu, C.-Y.: 2001, *J. Geophys. Res.* **106**, 8359.
- Marsch, E., Bourouaine, S.: 2011, *Annales Geophysicae* **29**, 2089.
- Matteini, L., Hellinger, P., Landi, S., Travnicek, P. M., Velli, M.: 2011, *Space Sci. Rev.* **172**, 737.
- Nariyuki, Y., Hada, T., Tsubouchi, K.: 2009, *J. Geophys. Res.* **114**, A07104.
- Nariyuki, Y., Hada, T., Tsubouchi, K.: 2012, *Phys. Plasmas* **19**, 082317.
- Osmane, A., Hamza, A. M., and Meziane, K.: 2010, *J. Geophys. Res.* **115**, A05101.
- Pierrard, V., Lazar, M., Schlickeiser R.: 2011, *Solar Phys.* **269**, 421.
- Pierrard, V., Maksimovic, M., Lemaire, J.: 1999, *J. Geophys. Res.* **104**, 17021.
- Pierrard, V., Voitenko, Y.: 2010, In: Maksimovic, M., Issautier, K., Meyer-Vernet, N., Moncuquet, M., Pantellini, F. (eds.), *Twelfth International Solar Wind Conference, AIP Conf. Proc.* **1216**, 102.
- Pierrard, V., Voitenko, Y.: 2012, *Solar Phys.*, accepted.
- Podesta, J. J., Gary, S. P.: 2011, *Astrophys. J.* **734**, 15.
- Rudakov, L., Mithaiwala, M., Ganguli, G., Crabtree, C.: 2011, *Phys. Plasmas* **18**, 012307.
- Rudakov, L., Crabtree, C., Ganguli, G., Mithaiwala, M.: 2012, *Phys. Plasmas* **19**, 042704.
- Sahraoui, F., Goldstein, M. L., Belmont, G., Canu, P., Rezeau, L.: 2010, *Phys. Rev. Lett.* **105**, id. 131101.
- Salem, C. S., Howes, G. G., Sundkvist, D., Bale, S. D., Chaston, C. C., Chen, C. H. K., Mozer, F. S.: 2012, *Astrophys. J. Lett.* **745**, L9.
- Schekochihin, A. A., Cowley, S. C., Dorland, W., Hammett, G. W., Howes, G. G., Quataert, E., Tatsuno, T.: 2009, *Astrophys. J. Suppl.* **182**, 310.
- Smith, C. W., Hamilton, K., Vasquez, B. J., and Leamon, R. J.: 2006, *Astrophys. J. Lett.* **645**, L85.
- Tu, C.-Y., Wang, L.-H., Marsch, E.: 2002, *J. Geophys. Res.* **107**, 1291.
- Valentini, F., Perrone, D., Veltri, P.: 2011, *Astrophys. J.* **739**, 54.
- Vocks, C., Mann, G.: 2009, *Astron. Astrophys.* **502**, 325.
- Voitenko, Yu. M.: 1998, *Solar Phys.* **182**, 411.
- Voitenko, Y., Goossens, M.: 2002, *Solar Phys.* **209**, 37.
- Voitenko, Y., Goossens, M.: 2003, *Space Sci. Rev.* **107**, 387.
- Voitenko, Y., Goossens, M.: 2006, *Space Sci. Rev.* **122**, 255.
- Voitenko, Y., De Keyser, Y.: 2011, *Nonlinear Proc. Geophys.* **18**, 587.
- Wu, D. J., Chen, L., Wu, C. S.: 2012, *Phys. Plasmas* **19**, 024511.
- Zhao, J. S., Wu, D. J., Lu, J. Y.: 2011, *Phys. Plasmas* **18**, 032903.